LUND UNIVERSITY

A seventh-Order Accurate and Stable Algorithm for the Computation of Stress Inside Cracked Rectangular Domains

Helsing, Johan; Jonsson, Anders

Published in:
International Journal for Multiscale Computational Engineering

DOI:
10.1615/IntJMultCompEng.v2.i1.40

2004

Link to publication

Citation for published version (APA):
Helsing, J., & Jonsson, A. (2004). A seventh-Order Accurate and Stable Algorithm for the Computation of Stress Inside Cracked Rectangular Domains. *International Journal for Multiscale Computational Engineering*, *2*(1), 47-68. https://doi.org/10.1615/IntJMultCompEng.v2.i1.40

Total number of authors:
2

General rights
Unless other specific re-use rights are stated the following general rights apply:
Copyright and moral rights for the publications made accessible in the public portal are retained by the authors and/or other copyright owners and it is a condition of accessing publications that users recognise and abide by the legal requirements associated with these rights.
• Users may download and print one copy of any publication from the public portal for the purpose of private study or research.
• You may not further distribute the material or use it for any profit-making activity or commercial gain
• You may freely distribute the URL identifying the publication in the public portal

Read more about Creative commons licenses: https://creativecommons.org/licenses/

Take down policy
If you believe that this document breaches copyright please contact us providing details, and we will remove access to the work immediately and investigate your claim.

LUND UNIVERSITY

PO Box 117
221 00 Lund
+46 46-222 00 00

A seventh order accurate and stable algorithm for the computation of stress inside cracked rectangular domains *

Johan Helsing † Anders Jonsson ‡

Abstract

A seventh order accurate and extremely stable algorithm for the rapid computation of stress fields inside cracked rectangular domains is presented. The algorithm is seventh order accurate since it incorporates basis functions taking the asymptotic shape of the stress fields close to crack tips and corners into account at least up to order six. The algorithm is stable since it is based on a Fredholm integral equation of the second kind. The particular form of the integral equation represents the the solution as the limit of a function which is analytic inside the domain. This allows for an efficient implementation. In an example, involving 112 discretization points on an elastic square with a center crack, values of normalized stress intensity factors and T-stress with a relative error of 10^{-6} are computed in seconds on a workstation. More points reduce the relative error down to 10^{-15}, where it saturates in double precision arithmetic. A large-scale setup with up to 1024 cracks in an elastic square is also studied, using up to 740,000 discretization points. The algorithm is intended as a basic building-block in general purpose solvers for fracture mechanics. It can also be used as a substitute for benchmark tables.

Key words: Stress analysis, polygonal domain, stress intensity factor, T-stress, cracks, integral equation of Fredholm type.

*This work was supported by NFR, TFR, and The Knut and Alice Wallenberg Foundation under TFR contracts 98-568 and 99-380.

†Numerical Analysis, Centre for Mathematical Sciences, Lund University, Box 118, SE-221 00 LUND, Sweden. Email: Johan.Helsing@na.lu.se, Phone: +46-(0)46-2223372.

‡Department of Solid Mechanics, Royal Institute of Technology, SE-100 44 Stockholm, Sweden.

1 INTRODUCTION

The accurate computation of stress fields inside polygonal domains, possibly containing inclusions and cracks, has traditionally been associated with substantial computing costs and stability problems. A large obstacle, irrespective of the numerical method used, is the difficulty of resolving the stress fields in the domain corners.

There are various ways to deal with corners. The easiest approach, which we refer to as 'brute force', is to represent the field in terms of polynomial basis functions and use a standard finite element or boundary element adaptive solver. This process is costly. Particularly so if high accuracy is required. Furthermore, as discretization points accumulate in the corners, the convergence may stop prematurely. Another approach is to use special basis functions which take the asymptotic (non-polynomial) form of the stress field in the corners into account. While special basis functions are economical in terms of discretization points, their inclusion into an algorithm easily add ill-conditioning to the problem.

Implementations of algorithms for the computation of stress fields inside polygonal domains are often of low order and aim at moderate accuracy. As we shall see, the results of different authors seldom agree to more than two or three digits, not even for simple setups. The purpose of this paper is to show that higher order accurate and stable schemes can and should be implemented. The conclusion is that with a careful choice of basis functions, with a careful implementation, and with a good formulation of the mathematical problem, one can construct schemes which are substantially more efficient than 'brute force'. Adaptivity may not even be necessary since for many problems, a few hundred discretization points give a solution whose quality is more than sufficient for engineering use.

Numerical results for an elastic rectangle with one or more cracks are presented. We construct a scheme which is approximately seventh order accurate both in theory and in practice. The scheme is extremely stable. With just a few hundred discretization points we compute stress intensity factors for an elastic rectangle with one crack with a relative error of only 10^{-7}. With two thousand points, or more, we decrease the relative error to less than $2 \cdot 10^{-15}$. A large-scale setup, involving up to 1024 slanted cracks in a uniaxially loaded square, is also studied using up to 740,000 discretization points. This demonstrates the capability of the scheme to handle large-scale problems.

2 PROBLEM STATEMENT AND POTENTIAL REPRESENTATION

A finite, linearly elastic, specimen occupies a domain D. The outer boundary of the specimen is denoted Γ_0 and is given positive (counter-clockwise) orientation. Inside the domain there are N_c cracks denoted Γ_k , $k = 1, 2, \ldots, N_c$. The domain D is therefore multiply connected. Crack k starts at crack tip $\gamma_{k\mathrm{s}}$ and ends at crack tip $\gamma_{k\mathrm{e}}$. The union of all cracks is Γ_c. The union of Γ_0 and Γ_c is Γ. The left and right sides of Γ are distinguished with superscripts $(+)$ and $(-)$. The exterior domain, outside Γ_0, is D'. Traction $(t_x^{\mathrm{pr}}, t_y^{\mathrm{pr}})$ is prescribed at Γ_0^+. The cracks are traction-free. We would like to compute the stress field in the entire plane.

Let $U(x, y)$ denote the Airy stress function. Since $U(x, y)$ satisfies the biharmonic equa-

tion everywhere, except for at Γ, it can be represented as

$$U(x,y) = \Re\mathrm{e}\left\{\bar{z}\phi(z) + \chi(z)\right\}\ , \tag{1}$$

where the potentials $\phi(z)$ and $\chi(z)$ are possibly multi-valued analytic functions of the complex variable $z = x + iy$. In the elasticity problem, requiring that the displacements be single-valued, see (11,12) below, and with certain conditions imposed on the applied external forces, see (19) below, $\phi(z)$ and $\chi'(z)$ are single-valued, see paragraph 40 of Mikhlin (1957). For a thorough discussion of the complex variable approach to elasticity problems, see Muskhelishvili (1953a), Sokolnikoff (1956), Mikhlin (1957), and Parton and Perlin (1982). The following relation links the complex potentials to the traction $t(z) = t_x(z) + it_y(z)$ along the tangent of a curve γ

$$t(z) = n\Phi(z) + n\overline{\Phi(z)} - \bar{n}z\overline{\Phi'(z)} - \bar{n}\overline{\Psi(z)}\,, \tag{2}$$

where $\Phi(z) = \phi'(z)$, $\Psi(z) = \chi''(z)$, and $n = n_x + in_y$ is the outward unit normal vector on γ.

The potentials $\Phi(z)$ and $\Psi(z)$ can be represented in the form of Cauchy-type integrals

$$\Phi(z) = \frac{1}{2\pi i}\int_\Gamma \frac{V(\tau)\,\mathrm{d}\tau}{(\tau - z)}\,, \quad z \in D \cup D'\,, \tag{3}$$

$$\Psi(z) = \frac{1}{2\pi i}\int_\Gamma \frac{W(\tau)\,\mathrm{d}\tau}{(\tau - z)}\,, \quad z \in D \cup D'\,, \tag{4}$$

where $V(\tau)$ and $W(\tau)$ are unknown layer densities on Γ. The representations for $\Phi(z)$ and $\Psi(z)$ of (3) and (4) guarantee that the equations of elasticity are satisfied everywhere in $D \cup D'$. It remains only to find $V(\tau)$ and $W(\tau)$, that is, to solve the boundary value problem

$$t(z) = t^{\mathrm{pr}}\,, \quad z \in \Gamma_0^+\,, \tag{5}$$

$$t(z) = 0\,, \quad z \in \Gamma_0^-\,, \tag{6}$$

$$t(z) = 0\,, \quad z \in \Gamma_c^+\,, \tag{7}$$

$$t(z) = 0\,, \quad z \in \Gamma_c^-\,, \tag{8}$$

where $t^{\mathrm{pr}} = t_x^{\mathrm{pr}} + it_y^{\mathrm{pr}}$ is the applied external traction.

3 TOWARDS AN EXTENDED MUSKHELISHVILI EQUATION

In this section we shall derive an integral equation for the stress problem stated in Section 2. The classic choice of integral equation for stress problems is the Sherman–Lauricella equation, see paragraph 56 of Mikhlin (1957). An alternative equation is presented in paragraph 98 of Muskhelishvili (1953a). The fundamental difference between the two equations is the choice of representation for the potential $\psi(z)$, related to $\Psi(z)$ via $\Psi(z) = \psi'(z)$.

The "Muskhelishvili equation" is often not recommended. Reasons are that the Sherman–Lauricella equation is considered simpler and more suitable for the purpose of general investigations (p. 398 of Muskhelishvili (1953a), 314 of Sokolnikoff (1956), and p. 255 of

Mikhlin (1957)), that the actual implementation of solutions to the Muskhelishvili equation for multiply connected domains is considered difficult because of the necessity of first solving auxiliary problems for some particular types of loading (p. 158 of Parton and Perlin (1982), and that the analysis of the Muskhelishvili equation for multiply connected domains is considerably more complicated (p. 249 of Mikhlin (1957)). Still, we observe, that for stress problems involving cracks, equations based on Muskhelishvili's choice of representation for $\psi(z)$ are often used, see paragraph 23 of Parton and Perlin (1982) and Section 6 of Chapter V in Parton and Perlin (1984).

We find it hard to determine which equation is the more difficult to analyze. Both the Sherman–Lauricella equation and the Muskhelishvili equation are difficult to deal with when it comes to proving uniqueness for multiply connected domains involving cracks. Especially so if the cracks are not straight. However, we find the Muskhelishvili equation so much more efficient than the Sherman–Lauricella equation, from a numerical point of view, that we shall use an extension of the Muskhelishvili equation in this paper. The problem of rigorously proving uniqueness will be left open.

We start with a useful lemma given in paragraph 36 of Muskhelishvili (1953a)

Lemma 3.1 *The solution to the plane problem of the theory of elasticity for z' in the external domain D' and with $t(z') = 0$ on Γ_0^- and displacements and stresses single-valued and bounded at infinity has the general solution $\Phi(z') = i\alpha$, where α is a real constant. When $\Phi(z')$ is represented as in (3), the solution is $\Phi(z') = 0$.*

According to Lemma 3.1, we shall seek $\Phi(z)$ as a function analytic inside D and zero in D'. To this end, we rewrite (3) as

$$\Phi(z) = \frac{1}{2\pi i}\int_{\Gamma_0} \frac{\Phi(\tau)\,\mathrm{d}\tau}{(\tau - z)} + \frac{1}{2\pi i}\int_{\Gamma_c} \frac{\Delta\Phi(\tau)\,\mathrm{d}\tau}{(\tau - z)}, \quad z \in D. \tag{9}$$

where $\Phi(\tau)$ is the limit of $\Phi(z)$ on Γ_0^+, and $\Delta\Phi(\tau)$ is the jump in $\Phi(z)$ over Γ_c (the limit on Γ_c^+ minus the limit on Γ_c^-). For z on Γ_0 equation (9) becomes

$$\Phi(z) = \frac{1}{\pi i}\int_{\Gamma_0} \frac{\Phi(\tau)\,\mathrm{d}\tau}{(\tau - z)} + \frac{1}{\pi i}\int_{\Gamma_c} \frac{\Delta\Phi(\tau)\,\mathrm{d}\tau}{(\tau - z)}, \quad z \in \Gamma_0. \tag{10}$$

To ensure that the displacements are single-valued we add the conditions

$$Q_0\Phi = 0, \tag{11}$$

$$Q_k\Delta\Phi = 0, \quad k = 1, 2, \ldots, N_c, \tag{12}$$

where where Q_j is a mapping from Γ_j to $\mathbb{C}$, defined by

$$Q_j f = \frac{1}{\pi i}\int_{\Gamma_j} f(\tau)\,\mathrm{d}\tau. \tag{13}$$

We now demand that the traction $t(z)$ of (2) jumps a quantity equal to the applied external traction as Γ_0 is crossed (conditions (5,6)), and that the traction $t(z)$ is continuous as Γ_c is crossed (conditions (7,8)). This, together with the representation (10), enable us to

express the density $W(\tau)$ of (4) in terms of $\Phi(\tau)$ and $\Delta\Phi(\tau)$. The potential $\Psi(z)$ assumes the form

$$\Psi(z) = -\frac{1}{2\pi i}\int_{\Gamma_0}\frac{\overline{\Phi(\tau)}\,\mathrm{d}\bar\tau}{(\tau-z)} - \frac{1}{2\pi i}\int_{\Gamma_0}\frac{\bar\tau\Phi(\tau)\,\mathrm{d}\tau}{(\tau-z)^2} - \frac{1}{2\pi i}\int_{\Gamma_0}\frac{\bar n\overline{t^{\mathrm{pr}}}\,\mathrm{d}\tau}{(\tau-z)}$$
$$-\frac{1}{2\pi i}\int_{\Gamma_c}\frac{\overline{\Delta\Phi(\tau)}\,\mathrm{d}\bar\tau}{(\tau-z)} - \frac{1}{2\pi i}\int_{\Gamma_c}\frac{\bar\tau\Delta\Phi(\tau)\,\mathrm{d}\tau}{(\tau-z)^2}\,, \qquad z\in D\cup D'\,. \tag{14}$$

The representation (14) for $\Psi(z)$ is the derivative of Muskhelishvili's representation for $\psi(z)$.

For brevity and simplicity, we assume that $N_c = 1$ in the following of this sections. The derivations can easily be generalized to the case when $N_c > 1$. The requirements (6,7) lead, via (2), to the following system of singular integral equations

$$\left(M_1^{(00)} - M_3^{(00)}\right)\Phi(z) + \left(M_1^{(01)} - M_3^{(01)}\right)\Delta\Phi(z) \tag{15}$$
$$= \frac{1}{2}\left(I - \frac{\bar n}{n}\overline{M_1}^{(00)}\frac{n}{\bar n}\right)\bar n t^{\mathrm{pr}}(z)\,, \quad z\in\Gamma_0\,,$$
$$\left(M_1^{(10)} - M_3^{(10)}\right)\Phi(z) + \left(M_1^{(11)} - M_3^{(11)}\right)\Delta\Phi(z) \tag{16}$$
$$= -\frac{1}{2}\frac{\bar n}{n}\overline{M_1}^{(10)}\frac{n}{\bar n}\bar n t^{\mathrm{pr}}(z)\,, \quad z\in\Gamma_1\,,$$

where the operator $M_1^{(jk)}$, acting on a function $f(z)$, is given by

$$M_1^{(jk)}f(z) = \frac{1}{\pi i}\int_{\Gamma_k}\frac{f(\tau)\,\mathrm{d}\tau}{(\tau-z)}\,, \quad z\in\Gamma_j\,, \tag{17}$$

the operator $\overline{M_1}^{(jk)}$ is the conjugate of $M_1^{(jk)}$, and the compact operator $M_3^{(jk)}$ is given by

$$M_3^{(jk)}f(z) = \frac{1}{2\pi i}\left[\int_{\Gamma_k}\frac{f(\tau)\,\mathrm{d}\tau}{(\tau-z)} + \frac{\bar n}{n}\int_{\Gamma_k}\frac{f(\tau)\,\mathrm{d}\tau}{(\bar\tau-\bar z)}\right. \tag{18}$$
$$\left. + \int_{\Gamma_k}\frac{\overline{f(\tau)}\,\mathrm{d}\bar\tau}{(\bar\tau-\bar z)} + \frac{\bar n}{n}\int_{\Gamma_k}\frac{(\tau-z)\overline{f(\tau)}\,\mathrm{d}\bar\tau}{(\bar\tau-\bar z)^2}\right]\,, \quad z\in\Gamma_j\,.$$

Equations (11,12,15,16) are not solvable unless the solvability conditions

$$P_0\bar n t^{\mathrm{pr}} = 0\,, \tag{19}$$
$$Q_0\bar n t^{\mathrm{pr}} = 0\,, \tag{20}$$

hold, where P_k is a mapping from Γ_k to $\mathbb{R}$, defined by

$$P_k f = -\frac{1}{2A}\Re\mathrm{e}\left\{\int_{\Gamma_k} f(z)\bar z\,\mathrm{d}z\right\}\,, \tag{21}$$

where A is the area of the domain D. Neither do (11,12,15,16) have a unique solution. The constant $\Phi_0(z) = i\alpha$, where α is real, is a homogeneous solution. We add the uniqueness condition

$$P_0\Phi = 0\,. \tag{22}$$

Since

$$P_0 i = 1\,, \tag{23}$$

equation (22) does not allow for the arbitrary addition of a homogeneous solution $\Phi_0(z) = i\alpha$ to $\Phi(z)$.

4 A FREDHOLM EQUATION OF THE SECOND KIND

Equations (15,16) are singular Fredholm integral equations of the first kind. Upon discretization such equations lead to systems of linear equations whose condition numbers grow with increased resolution. Implementing the conditions (11,12,22) may also pose problems. These equations are therefore not good for numerics. In this section we shall reformulate the five equations (11,12,15,16,22) and arrive at a system of two second kind Fredholm integral equations that is well suited for computations. We assume that $N_c = 1$ for reasons of simplicity and brevity. All derivations are easy to modify for cases when $N_c > 1$.

First we shall combine (15) and (22) into a single equation. The following lemma is useful

Lemma 4.1 *Changing the order of integration, and using partial integration, one can show*

$$P_0 \left[\left(M_1^{(00)} - M_3^{(00)} \right) \Phi(z) + \left(M_1^{(01)} - M_3^{(01)} \right) \Delta\Phi(z) \right] \Omega = 0\,, \tag{24}$$

$$P_0 \frac{1}{2} \left(I - \frac{\bar{n}}{n} \overline{M_1}^{(00)} \frac{n}{\bar{n}} \right) \bar{n} t^{\mathrm{pr}} = P_0 \bar{n} t^{\mathrm{pr}}, \tag{25}$$

whatever the applied traction t^{pr} is.

Now a linear combination of (15) and (22) gives

$$\begin{aligned} \left(M_1^{(00)} - M_3^{(00)} + iP_0 \right) \Phi(z) + \left(M_1^{(01)} - M_3^{(01)} \right) \Delta\Phi(z) \\ = \frac{1}{2} \left(I - \frac{\bar{n}}{n} \overline{M_1}^{(00)} \frac{n}{\bar{n}} \right) \bar{n} t^{\mathrm{pr}}(z)\,, \quad z \in \Gamma_0\,, \end{aligned} \tag{26}$$

To show that (26) is equivalent to (15,22), assuming that (19) holds, we apply P_0 from the left in (26). This gives (22) with the help of Lemma 4.1 and (19,23). A linear combination of (22) and (26) gives back (15).

Next we make use of (10) and rewrite (26) as a second kind equation

$$\begin{aligned} \left(I - M_3^{(00)} + iP_0 \right) \Phi(z) - M_3^{(01)} \Delta\Phi(z) \\ = \frac{1}{2} \left(I - \frac{\bar{n}}{n} \overline{M_1}^{(00)} \frac{n}{\bar{n}} \right) \bar{n} t^{\mathrm{pr}}(z)\,, \quad z \in \Gamma_0\,. \end{aligned} \tag{27}$$

To show that (27) is equivalent to (26) we must prove that (27) does not allow for a homogeneous solution whose analytic extension to the plane is non-zero in D'. We therefore investigate solutions to the homogeneous equation

$$\left(I - M_3^{(00)} + iP_0 \right) \Phi_0(z) - M_3^{(01)} \Delta\Phi_0(z) = 0\,, \quad z \in \Gamma_0\,. \tag{28}$$

Using the new analytic functions in D'

$$\Phi^*(z') = -\frac{P_0\Phi_0}{2} - \frac{1}{2\pi}\int_{\Gamma_0}\frac{\Phi_0(\tau)\,\mathrm{d}\tau}{(\tau - z')} - \frac{1}{2\pi}\int_{\Gamma_c}\frac{\Delta\Phi_0(\tau)\,\mathrm{d}\tau}{(\tau - z')}\,, \quad z' \in D'\,, \tag{29}$$

and

$$\Psi^*(z') = \frac{1}{2\pi}\int_{\Gamma_0}\frac{\overline{\Phi_0(\tau)}\,\mathrm{d}\bar{\tau}}{(\tau - z')} + \frac{1}{2\pi}\int_{\Gamma_0}\frac{\bar{\tau}\Phi_0(\tau)\,\mathrm{d}\tau}{(\tau - z')^2} \tag{30}$$

$$+\frac{1}{2\pi}\int_{\Gamma_c}\frac{\overline{\Delta\Phi_0(\tau)}\,\mathrm{d}\bar{\tau}}{(\tau - z')} + \frac{1}{2\pi}\int_{\Gamma_c}\frac{\bar{\tau}\Delta\Phi_0(\tau)\,\mathrm{d}\tau}{(\tau - z')^2}\,, \quad z' \in D'\,,$$

and taking limits, one can show

$$\lim_{z'\to\Gamma_0^-} n\Phi^*(z') + n\overline{\Phi^*(z')} - \bar{n}z'\overline{\Phi^{*\prime}(z')} - \bar{n}\overline{\Psi^*(z')} \tag{31}$$

$$= in\left(I - M_3^{(00)} + iP_0\right)\Phi_0(z) - inM_3^{(01)}\Delta\Phi_0(z)\,, \quad z = \lim z' \to \Gamma_0^-\,.$$

Now the equation

$$\lim_{z'\to\Gamma_0^-} n\Phi^*(z') + n\overline{\Phi^*(z')} - \bar{n}z\overline{\Phi^{*\prime}(z')} - \bar{n}\overline{\Psi^*(z')} = 0\,, \tag{32}$$

has, according to Lemma 3.1, only the solution $\Phi^*(z') = i\alpha$. The form of the representation (29) implies that $\Phi^*(z') = 0$ for $z' \in D'$, and therefore $\Phi_0(z)$ on Γ has to be the limit of a function analytic in D and zero in D'.

For the transformation of the entire system (11,12,16,27) into second kind equations we need to introduce a weight $\rho(z)$ which for $z \in \Gamma_k$ is given by

$$\rho(z) = \begin{cases} 1, & k = 0, \\ ((z-\gamma_{k\mathrm{s}})(z-\gamma_{k\mathrm{e}}))^{-\frac{1}{2}}, & k = 1, 2, \ldots, N_c\,. \end{cases} \tag{33}$$

To be precise, the weight $\rho(z)$ is the limit from the right (relative to the orientation of crack k) of the branch given by a branch cut along Γ_k and

$$\lim_{z\to\infty} z\rho(z) = 1. \tag{34}$$

We also introduce the new, smooth, unknown function $\Omega(z)$ via the substitution

$$\rho(z)\Omega(z) = \Phi(z)\,, \quad z \in \Gamma_0\,, \tag{35}$$

$$\rho(z)\Omega(z) = \Delta\Phi(z)\,, \quad z \in \Gamma_c\,. \tag{36}$$

The system of equations (11,12,16,27) now reads

$$\left(I - M_3^{(00)} - M_3^{(01)}\rho + iP_0\right)\Omega(z) = \frac{1}{2}\left(I - \frac{\bar{n}}{n}\overline{M_1}^{(00)}\frac{n}{\bar{n}}\right)\bar{n}t^{\mathrm{pr}}(z)\,, \quad z \in \Gamma_0\,. \tag{37}$$

$$\left(M_1^{(10)} - M_3^{(10)} + M_1^{(11)}\rho - M_3^{(11)}\rho\right)\Omega(z) \tag{38}$$

$$= -\frac{1}{2}\frac{\bar{n}}{n}\overline{M_1}^{(10)}\frac{n}{\bar{n}}\bar{n}t^{\mathrm{pr}}(z)\,, \quad z \in \Gamma_1\,,$$

$$Q_0\rho\Omega = 0\,, \tag{39}$$

$$Q_k\rho\Omega = 0\,, \quad k = 0, 2, \ldots, N_c\,. \tag{40}$$

It was shown in Helsing and Peters (1999) that the following relations involving Q_1, $\rho(z)$, and $M_1^{(11)}$ hold

Lemma 4.2

$$Q_1\rho M_1^{(11)}\rho^{-1}f(z) = 0\,, \tag{41}$$

$$M_1^{(11)}\rho^{-1}M_1^{(11)}\rho f(z) = f(z) - Q_1\rho f\,, \quad z \in \Gamma_1\,, \tag{42}$$

$$M_1^{(11)}\rho M_1^{(11)}\rho^{-1}f(z) = f(z)\,, \quad z \in \Gamma_1\,, \tag{43}$$

where $f(z)$ is a square integrable function. See also p. 155 of Estrada and Kanwal (2000).

It is now easy to show that the system (37-40) is equivalent to the following two integral equations of Fredholm's second kind

$$\left(I - M_3^{(00)} - M_3^{(01)}\rho + iP_1\right)\Omega(z) = \frac{1}{2}\left(I - \frac{\bar{n}}{n}\overline{M_1}^{(00)}\frac{n}{\bar{n}}\right)\bar{n}t^{\mathrm{pr}}(z)\,, \quad z \in \Gamma_0\,. \tag{44}$$

$$\left(I + M_1^{(11)}\rho^{-1}\left(M_1^{(10)} - M_3^{(10)} - M_3^{(11)}\rho\right)\right)\Omega(z) \tag{45}$$

$$= -M_1^{(22)}\rho^{-1}\frac{1}{2}\frac{\bar{n}}{n}\overline{M_1}^{(10)}\frac{n}{\bar{n}}\bar{n}t^{\mathrm{pr}}(z)\,, \quad z \in \Gamma_c\,.$$

Application of $M_1^{(11)}\rho^{-1}$ from the left in (38) and the use of (40) and the relation (42) give (45). In the other way we apply $Q_1\rho$ to the left in (45). The relation (41) gives back (40). Application of $M_1^{(11)}\rho$ to the left in (45) and the relation (43) give back (38). Application of Q_0 to the left in (44) and use of (20,40) give back (39).

Equations (44,45) will be used for computations in Section 10. We end this section with a listing of some particular advantages with these equations and their solution $\Omega(z)$.

- Equations (44,45) are of Fredholm's second kind with compact operators. This allows for stable convergence as the system is discretized and solved on an increasingly refined mesh. See Helsing and Peters(1999) for proof that the composition of integral operators in (45) are compact.

- The density $\Omega(z)$ on Γ_0 is the limit of $\Phi(z)$ in D. This simplifies the construction of an asymptotically correct basis for $\Omega(z)$ in the corners. The action of the integral operators can be implemented in an efficient way. See Sections 6 and 8.

- The density $\Omega(z)$ is simply related to $\Phi(z)$ and $\Psi(z)$ and therefore also to the stress in D, see Section 5. The solutions to the original Muskhelishvili- and Sherman–Lauricella equations are related to the potentials $\phi(z)$ and $\psi(z)$. The stress has to be computed via differentiation, which is an ill-conditioned operation. See also p. 92 in Section 6 of Chapter V of Parton and Perlin (1984) for a discussion of these matters.

- Equation (44) contains the operator P_1 which removes an indeterminacy in $\Phi(z)$. The original Muskhelishvili- and Sherman–Lauricella equations contains other operators which remove a larger indeterminacy in $\phi(z)$ and involve an arbitrarily placed point. An unfortunate placement of this point could degrade numerical performance. Generally, the operator P_0 seem to lead to more stable schemes, see Helsing (2000).

- A recent trend in the development of integral equations for planar elasticity is to work with Green's functions for stresses and displacements. This is referred to as "standard BEM", see Becker (1992). Disadvantages with the BEM equations are that they solve for displacement fields, that they involve logarithmic kernels, and that they seem less economical for crack and inclusion problems.

5 EXTRACTION OF STRESS AND STRESS INTENSITY FACTORS

Once (44,45) are solved for $\Omega(z)$, the potentials $\Phi(z)$ and $\Psi(z)$ can be computed everywhere in D via (9,14,35,36). This enables the rapid extraction of many quantities of physical interest. Here we list a few.

The components of the stress tensor in the material are always of interest. They can be computed via

$$\sigma_{xx} + \sigma_{yy} = 4\Re\mathrm{e}\{\Phi(z)\}\,, \tag{46}$$

$$\sigma_{yy} - \sigma_{xx} - 2i\sigma_{xy} = 2(z\overline{\Phi'(z)} + \overline{\Psi(z)})\,. \tag{47}$$

A function of the stresses, which is used to predict the occurrence of yielding in a material where the stress state is multiaxial, is the von Mises effective stress σ_{e}. For plane strain conditions, it can be expressed as

$$\sigma_{\mathrm{e}} = \left[(1-\nu(1-\nu))\,(\sigma_{xx}+\sigma_{yy})^2 - 3\left(\sigma_{xx}\sigma_{yy} - \sigma_{xy}^2\right)\right]^{1/2}\,, \tag{48}$$

where ν is the Poisson's ratio.

Linear elastic fracture mechanics is widely used to predict the fracture resistance of cracked structures. Linear theory has been successful even though non-linear material behavior occurs in regions close to crack tips. The reason for this is the small scale yielding assumption, which states that the fracture process is governed by so-called stress intensity factors whenever the plastic zone is small compared to other specimen dimensions. The assumption is assumed to hold if $l > 2.5(K_{Ic}/\sigma_Y)^2$, where l is the smallest characteristic length of the specimen, K_{Ic} is the fracture toughness of the material and σ_Y is the tensile yield strength of the material (ATSM (1998)). The stress intensity factors can then be used to estimate the extent of the plastic zone. The complex valued stress intensity factor $K = K_I + iK_{II}$ at the crack tips $\gamma_{k\mathrm{s}}$ and $\gamma_{k\mathrm{e}}$ can be defined as

$$K(\gamma_{k\mathrm{s}}) = \lim_{\epsilon\to 0^+} \sqrt{2\pi\epsilon}\left[\sigma_{y'y'}(\gamma_{k\mathrm{s}} - i\epsilon n_{\mathrm{s}}) + i\sigma_{x'y'}(\gamma_{k\mathrm{s}} - i\epsilon n_{\mathrm{s}})\right]\,, \tag{49}$$

$$K(\gamma_{k\mathrm{e}}) = \lim_{\epsilon\to 0^+} \sqrt{2\pi\epsilon}\left[\sigma_{y'y'}(\gamma_{k\mathrm{e}} + i\epsilon n_{\mathrm{e}}) + i\sigma_{x'y'}(\gamma_{k\mathrm{e}} + i\epsilon n_{\mathrm{e}})\right]\,, \tag{50}$$

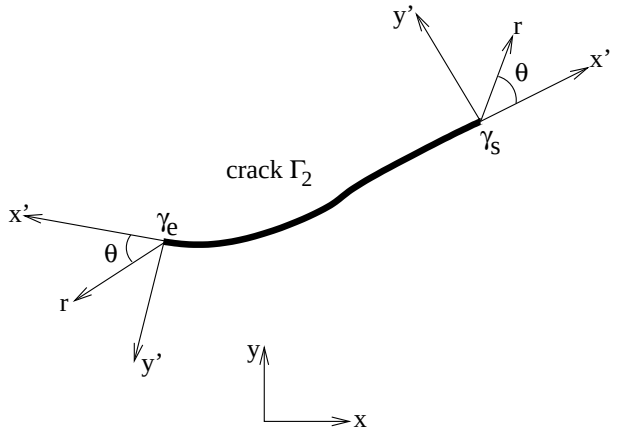

Figure 1: Local coordinate systems aligned with the tangent to the crack at the crack tips.

where ϵ is a real number, $n_{\mathrm{s}} = n(\gamma_{k\mathrm{s}})$, $n_{\mathrm{e}} = n(\gamma_{k\mathrm{e}})$, and x', y' refer to local coordinate systems parallel to the tangent of the crack at the crack tips, see Figure 1. A normalized stress intensity factor $F = F_{\mathrm{I}} + iF_{\mathrm{II}}$ is introduced as

$$F = \frac{K}{t_y^{\mathrm{pr}}\sqrt{\pi a}}\,, \tag{51}$$

where t_y^{pr} is the applied external load and a is half the length of an internal crack or the entire length of an edge crack. The normalized stress intensity factor can be computed as

$$F(\gamma_{k\mathrm{s}}) = \frac{i\sqrt{2}}{t_y^{\mathrm{pr}}\sqrt{a}} \lim_{z\to\gamma_{k\mathrm{s}}} \overline{\Omega(\gamma_{k\mathrm{s}})\rho(z)}\sqrt{\delta s(z)}\,, \qquad z \in \Gamma_k\,, \tag{52}$$

$$F(\gamma_{k\mathrm{e}}) = -\frac{i\sqrt{2}}{t_y^{\mathrm{pr}}\sqrt{a}} \lim_{z\to\gamma_{k\mathrm{e}}} \overline{\Omega(\gamma_{k\mathrm{e}})\rho(z)}\sqrt{\delta s(z)}\,, \qquad z \in \Gamma_k\,, \tag{53}$$

where $\delta s(z)$ is arclength measured from the closest crack tip.

Larsson and Carlsson (1973) studied four common test specimen geometries and showed that stress intensity factors alone are not sufficient to determine the extent of the plastic zones around the crack tips. They suggested that the first non-singular, constant, term in the series expansion of the normal stress parallel to the crack-plane, at the crack tips, should also be considered. This term is referred to as T-stress. Betegón and Hancock (1991) went further and concluded that the crack tip field will be dominated by the stress intensity factors K if T is positive. The K-dominance is lost for negative T. This implies that if T is negative, it should be included as a parameter in fracture resistance estimation. If T is positive, it can be neglected and the small scale yielding assumption is valid. In order to correctly predict the fracture toughness of a structure, the same level of negative T-stress should therefore be used in tests as is present in a real situation. Today, including effects of the T-stress in tests is a relatively well established procedure, at least in mode I fracture, see Hallbäck (1996). The real valued T-stress at crack tips $\gamma_{k\mathrm{s}}$ and $\gamma_{k\mathrm{e}}$ can be defined as

$$T(\gamma_{k\mathrm{s}}) = \lim_{\epsilon\to 0^+} \sigma_{x'x'}(\gamma_{k\mathrm{s}} - i\epsilon n_{\mathrm{s}}) - \sigma_{y'y'}(\gamma_{k\mathrm{s}} - i\epsilon n_{\mathrm{s}})\,, \tag{54}$$

$$T(\gamma_{k\mathrm{e}}) = \lim_{\epsilon \to 0^+} \sigma_{x'x'}(\gamma_{k\mathrm{e}} + i\epsilon n_{\mathrm{e}}) - \sigma_{y'y'}(\gamma_{k\mathrm{e}} + i\epsilon n_{\mathrm{e}}) \,, \tag{55}$$

In terms of complex potentials these expression assume the form

$$T(\gamma_{kj}) = 2\Re\mathrm{e}\left\{\frac{\bar{n}}{n}\left(\gamma_{kj}\overline{\Phi'(\gamma_{kj})} + \overline{\Psi(\gamma_{kj})}\right)\right\} \,, \quad j = \mathrm{s}, \mathrm{e} \,. \tag{56}$$

For straight cracks, the expression (56) can be evaluated as

$$T(\gamma_{kj}) = 2\Re\mathrm{e}\left\{\sum_{m=0}^{N_c} M_3^{(km)} \rho\Omega(\gamma_{kj}) - \frac{1}{2}\frac{\bar{n}}{n}\overline{M_1}^{(k0)}\frac{n}{\bar{n}}\bar{n}t^{\mathrm{pr}}(\gamma_{kj})\right\} \,, \quad j = \mathrm{s}, \mathrm{e} \,. \tag{57}$$

The biaxiality parameter B is introduced by normalizing the T-stress. For uniaxial applied traction in the y-direction the normalization reads

$$B = \frac{T}{t_y^{\mathrm{pr}}\sqrt{F_{\mathrm{I}}^2 + F_{\mathrm{II}}^2}} \,. \tag{58}$$

We shall now devote the four following sections to the implementation of a seventh order accurate algorithm for the solution of (44,45).

6 SMOOTH AND NON-SMOOTH FUNCTIONS

The accuracy of a particular implementation of an integral operator will depend on the continuity properties of the function on which the operator is acting. This section discusses the smoothness of the function $\Omega(z)$ and t^{pr} appearing in (44,45).

The density $\Omega(z)$ is a smooth function (C^∞) on Γ_c. This is so thanks to the introduction of the weight $\rho(z)$ of (33). The applied traction t^{pr} is also smooth, but discontinuous in the corners. The density $\Omega(z)$ on Γ_0, on the other hand, is not smooth. In the corners, $\Omega(z)$ can be decomposed into a symmetric part and an antisymmetric part containing terms of the form

$$\Omega_{\mathrm{symm}}(z) = c_{\mathrm{s}} z^{\lambda-1} + \bar{c}_{\mathrm{s}} z^{\bar{\lambda}-1} \,, \tag{59}$$

and

$$\Omega_{\mathrm{antisymm}}(z) = c_{\mathrm{as}} z^{\mu-1} - \bar{c}_{\mathrm{as}} z^{\bar{\mu}-1} \,, \tag{60}$$

where c_{s} and c_{as} are complex coefficients and where λ and μ are a mix of positive integer exponents and widely spaced non-integer exponents given by the Williams solution, see Williams (1952). The special case of real λ and μ renders c_{s} real and c_{as} purely imaginary. See Helsing and Jonsson (2001) for details. In this paper we shall use integer values of λ and μ ranging from one to six, together with the first non-integer values in the Williams series for λ and μ. The first omitted term in the Williams series for λ has a real part of approximately 6.845. The first omitted term in the Williams series for μ has a real part of approximately 8.87.

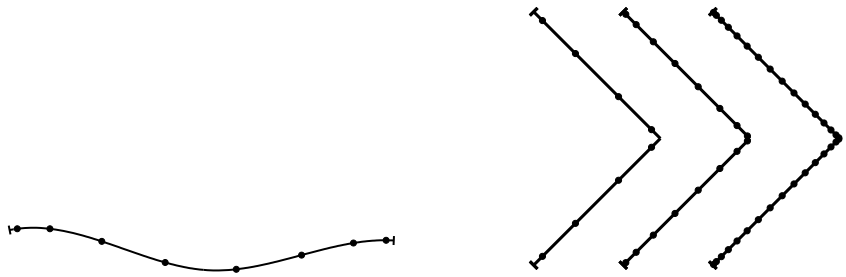

Figure 2: Left, a regular quadrature panel. Right, corner quadrature panels with two legs. The dots on the regular panel and on the leftmost corner panel symbolize points where the solution Ω has support. The other two corner panels show points where intermediate quantities are computed.

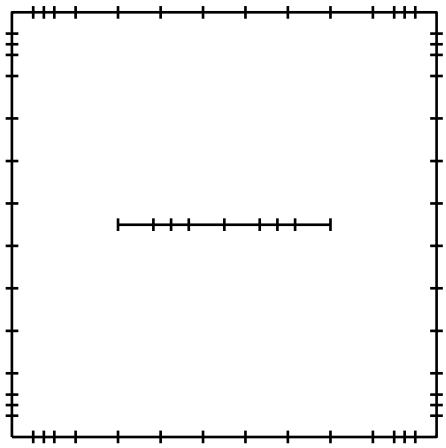

Figure 3: Quadrature panels on a modified uniform mesh for a square with a centered crack. Most panels have the same length. Panels neighboring to corner panels and panels neighboring to panels containing crac-tips are shorter.

7 DISCRETIZATION AND BASIC QUADRATURE

We intend to solve (44,45) using a Nyström scheme with composite eight-point Gauss-Legendre quadrature as our basic quadrature rule. On panels containing crack tips we use eight-point Gauss-Jacobi quadrature. To this end we divide Γ_0 and Γ_c into quadrature panels. First we let all panels have approximately the same length. This construction we call a standard uniform mesh. We arrange the panels so that all four corners are symmetrically included in panels referred to as corner panels, see Figure 2. Panels which do not contain corners are referred to as regular panels. We now perform a modification of the standard uniform mesh. If a regular panel is neighboring to a panel containing a crack tip, it is subdivided once into two smaller regular panels. If a regular panel is neighboring to a corner panel, it is subdivided twice into three smaller regular panels with the two smallest panels closest to the corner panel. We call the resulting mesh a modified uniform mesh. See Figure 3.

There are two reasons for using the modified uniform mesh rather than the standard uniform mesh. The first reason has to do with that the solution $\Omega(z)$ on regular panels close to a corner varies faster than further away from the corner. Although $\Omega(z)$ is smooth on panels neighboring to corners, a certain singular-like behavior can be discerned. Should a standard uniform mesh be refined, the solution $\Omega(z)$ on regular panels neighboring to corners will vary even faster and the its quality would not necessarily be improved. A similar effect is present for $\Omega(z)$ on panels close to crack tips. The density $\Omega(z)$ is smooth on the entire crack Γ_c thanks to the weight $\rho(z)$. Unfortunately, $\rho(z)$ cannot be used as a quadrature weight in the composite quadrature scheme. We implement the quadrature on the panels of Γ_c using the following reformulation, where f is a smooth function,

$$\int_a^b \rho(\tau) f(\tau)\,\mathrm{d}\tau = \int_{t_a}^{t_b} \frac{\rho(\tau)}{h(t)} f(\tau) \frac{\mathrm{d}\tau}{\mathrm{d}t} h(t)\,\mathrm{d}t\,. \tag{61}$$

In (61) t is a parameterization and $h(t)$ is a real valued weight incorporated into the quadrature. If $a = \gamma_{k\mathrm{s}}$ we choose $h(t) = 1/\sqrt{t - t_a}$. If $b = \gamma_{k\mathrm{e}}$ we choose $h(t) = 1/\sqrt{t_b - t}$. If neither a nor b are crack tips we choose $h(t) = 1$. In this way we get high precision on panels containing crack tips and panels not neighboring to crack tips. On panels that do neighbor to crack tips the factor $\rho(\tau)/h(t)$ will grow as a standard uniform mesh is refined. Full double precision accuracy for the quadratures cannot be achieved.

The second reason for using the modified uniform mesh rather than the standard uniform mesh has to do with the interaction between neighboring panels on opposite sides of corners. When a standard uniform mesh is refined, neighboring panels on opposite sides of a corner are moving closer to each other and are simultaneously shrinking. The net effect may be that the integral kernels describing these interactions is never well resolved. Numerical experiments indicate that refinement of a modified uniform mesh will allow us to reach double precision accurate answers.

As for the placement of discretization points we do as follows: on all regular panels we place eight Gauss-Legendre nodes for the support of $\Omega(z)$. On panels containing crack tips we place eight Gauss-Jacobi nodes for the support of $\Omega(z)$. On each leg of the corner panels we place one set of four Gauss-Legendre for the support of $\Omega(z)$. Also, on each leg of the corner panels we place one set of eight Gauss-Legendre nodes and one set of sixteen Gauss-Legendre nodes. See Figure 2. On these extra sets of nodes, intermediate quantities will have support. We shall thus use three sets of nodes on corner panels for different purposes in our implementation of the operators appearing in (44,45). The overall ambition is that all quadratures shall be implemented with at least seventh order accuracy.

8 IMPLEMENTATION OF INTEGRAL OPERATORS

8.1 Review of previous implementations

The implementation of several of the operators appearing in (44,45) have been discussed in previous work. The implementation of other operators can be done in similar ways. Here follows a brief review. Once again, for brevity, details will only be given for the case $N_c = 1$. Extensions are analogous.

The implementation of the operators $M_3^{(01)}\rho$, $M_3^{(11)}\rho$, and $M_1^{(11)}\rho^{-1}$ for action on smooth functions are discussed in Helsing and Peters (1999). The implementation of $M_3^{(01)}\rho$ and

$M_3^{(11)}\rho$ will be 16th order accurate with eight Gauss-Legendre or Gauss-Jacobi nodes as source points. The implementation of $M_1^{(11)}\rho^{-1}$ will be eighth order accurate. With nth order accuracy we mean that a polynomial of order $n-1$ can be integrated exactly.

The implementation of $M_3^{(00)}$ for action on the non-smooth function $\Omega(z)$ is rather involved. It is discussed in detail in Helsing and Jonsson (2001). In short, the operator $M_3^{(00)}$ is decomposed into three parts. One part of $M_3^{(00)}$ describes the action on $\Omega(z)$ for source points on regular panels. Here 16th order Gauss-Legendre quadrature is used. Another part of $M_3^{(00)}$ describes the action on $\Omega(z)$ for source points on corner panels and target points close to the source points. Here a change of basis for $\Omega(z)$, from pointwise representation to a representation in terms of the basis functions of (59,60), is used. The values of the different entries of the matrix representing this part of $M_3^{(00)}$ are precomputed to high precision using adaptive quadrature. The accuracy of the scheme is of order 6.845. The third part of $M_3^{(00)}$ describes the action on $\Omega(z)$ for source points on corner panels and target points far away from the source points. Here, too, a change of basis is employed, followed by interpolation and 32nd order accurate quadrature. The intermediate set of 16 quadrature points on each corner leg is used in this procedure whose accuracy is estimated to, again, 6.845. The decision of whether a target point should be considered being close to or far away from a corner panel will of course affect the achievable accuracy of the implementation of $M_3^{(00)}$. Numerical experiments indicate that, with our modified uniform mesh and for double precision accuracy, it is generally sufficient to consider points on the six closest panels neighboring to a corner leg as being close to the corner panel.

The implementation of $M_1^{(10)}$ and $M_3^{(10)}$ for action on $\Omega(z)$ resembles the implementation of $M_3^{(00)}$. The only difference is that the second part in the decomposition, for the action on source points on corner panels and target points close to the source points, is not needed.

8.2 Implementation of $M_1^{(00)}$ and $M_1^{(10)}$

We now discuss an eighth order accurate implementation of the operator $M_1^{(00)}$ whose conjugate acts on the applied traction in (44). The traction will be evaluated at all nodes on regular panels and on the intermediate sets of eight nodes on the legs of corner panels.

The operator $M_1^{(00)}$ is singular. The part of $M_1^{(00)}$ that describes action on source points on one quadrature panel when target points are on another panels is, however, compact. We use 16th order Gauss-Legendre quadrature for this action whenever the source points are on a regular panel and the target points are on a panel far away from that panel. Three panel lengths can be considered "far away" for double precision accuracy.

The implementation of $M_1^{(00)}$ for action on a function $f(z)$ when source points are on a regular panel and when target points are close to or on that panel is evaluated using the following relation. Let $f(z)$ be smooth and let a and b be the starting point and the endpoint of a regular quadrature panel. Then

$$\frac{1}{\pi i}\int_a^b \frac{f(\tau)\,\mathrm{d}\tau}{(\tau-z)} = \frac{1}{\pi}\int_a^b f(\tau)\Re\mathrm{e}\left\{\frac{\mathrm{d}\tau}{i(\tau-z)}\right\}$$

$$+\frac{i}{\pi}\int_a^b (f(\tau)-f(z))\Im\mathrm{m}\left\{\frac{\mathrm{d}\tau}{i(\tau-z)}\right\} + \frac{f(z)}{\pi i}\Re\mathrm{e}\left\{\ln\left[\frac{a-z}{b-z}\right]\right\}. \tag{62}$$

The first integral on the right hand side of (62) has a smooth kernel. The second integral has a smooth integrand. The third term is easy to evaluate.

The implementation of $M_1^{(00)}$ for action on a function $f(z)$ when source points are on a corner panel and when target points are close to or on that panel is dealt with as follows: It is assumed that $f(z)$ is available on eight Legendre nodes on each corner leg. A Legendre transform of $f(z)$ is computed. Legendre transforms are very stable. Then terms are recombined in the Legendre expansion as to get the coefficients in a monomial basis for $f(z)$. Finally the action of $M_1^{(00)}$ on each term in the monomial basis is evaluated analytically. This procedure is eighth order accurate. The parts of $M_1^{(00)}$ that describe the action on $f(z)$ on a leg of a corner panel when target points are far away from that leg are computed with eighth order accurate quadrature based on the values of $f(z)$ at the set of four nodes on each leg.

The operator $M_1^{(10)}$ is compact but its implementation is complicated by the fact that it is acting both on $\Omega(z)$, which is non-smooth, and on the prescribed traction, which is smooth. For the smooth action, we discretize using Gauss-Legendre quadrature in all points where $\Omega(z)$ has support. This procedure is ninth order accurate. For the non-smooth action, we implement $M_1^{(10)}$ like $M_3^{(10)}$ and the accuracy is the same.

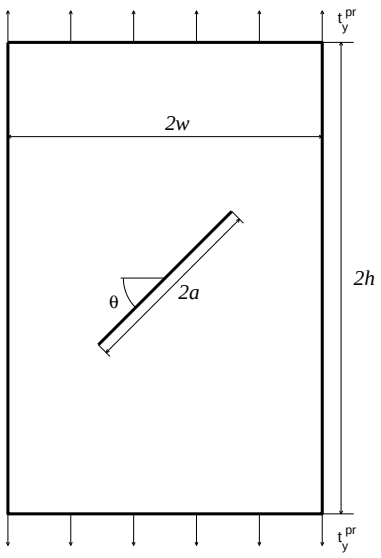

Figure 4: An elastic rectangle of height $2h$ and width $2w$ with a centered crack of length $2a$. The crack is slanted with an angle θ. A uniform external traction t_y^{pr} of unit strength is applied to two opposite sides of the rectangle. The other two sides of the rectangle are traction-free.

9 THE ALGORITHM

We discretize (44,45) with N points as outlined in the previous sections. Our geometry is a rectangle of height $2h$ and width $2w$. Inside the rectangle there is either one or more straight crack of length $2a$, see Figure 4 and Figure 5, or a circular arc-shaped crack of radius R. A few things can be noted.

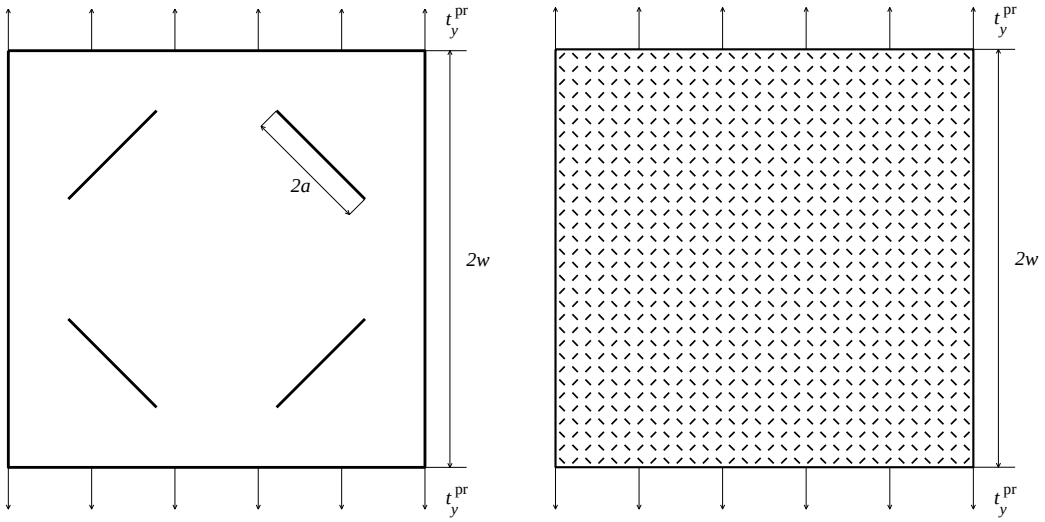

Figure 5: Two setups with multiple cracks. The square plate has side lengths $2w$ and contains $4m^2$ straight slanted cracks with angle $\pi/4$ and length $2a = 0.6w/m$. The cracks are placed on a square grid with a distance w/m between grid points. Distances between crack mid-points are $w/(2m)$.The left plate has $m = 1$ and the right has $m = 16$.

- For a straight crack, $M_3^{(11)}$ vanishes and (45) simplifies.
- The implementation of $M_1^{(10)}$ is dependent on whether the operator is acting on a smooth function or not. Only parts which describe action on corner panels are computed and stored twice.
- The GMRES solver (Saad and Schultz (1986)) is used for the system of linear equations. The iterations are terminated when the relative norm of the residual is as small as it can get. This often means 10^{-16}. The number of iterations needed for convergence, given a geometry and a load, is almost independent of the number of discretization points. This is typical for discretized Fredholm integral equations of the second kind.
- Great care is devoted to avoiding roundoff error throughout the code. Matrix-vector multiplications and inner products are evaluated with compensated summation, se Higham (1996) and Kahan (1965), for the small-scale examples. The fast multipole method, see Helsing and Greengard (1998), and Greengard and Rokhlin (1987), is used for large-scale computations.
- The operators of (44,45) are implemented with order of accuracies ranging from 6.845 to 16. We expect the asymptotic convergence rate to be of order 6.845, which is indistinguishable from seven in double precision accuracy.
- The complexity and storage requirement of our implementation grows as N^2 for the small-scale examples. By use of the fast multipole method for the large-scale examples, the complexity and the storage requirement is proportional to N.

10 NUMERICAL EXAMPLES

The purpose of this section is to demonstrate the extreme stability of our scheme. Three small-scale examples are studied for this purpose. In a fourht example, we demonstrate the capability of our scheme to handle large-scale computations.

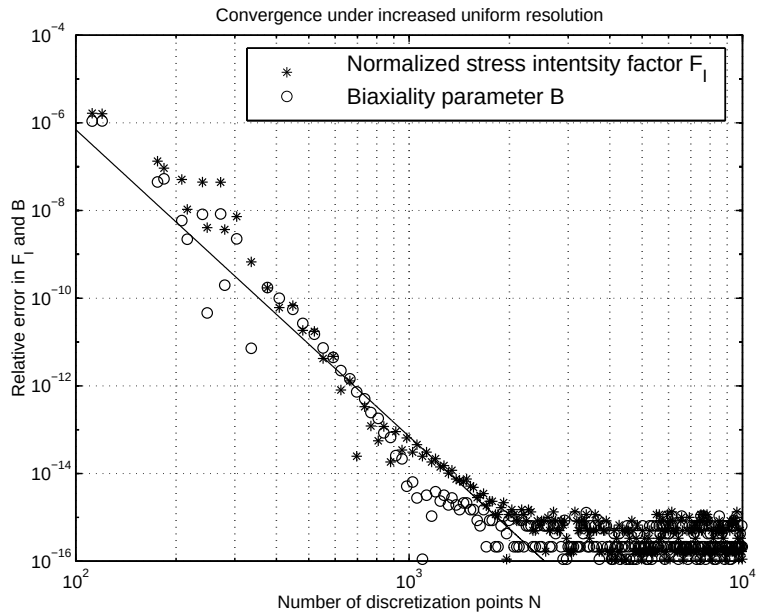

Figure 6: Convergence of normalized stress intensity factor F_{I} of (52) and biaxiality parameter B of (58) at the tips of a a centered crack of length $2a = 0.5$ in a unit square under unit uniform uniaxial load. A modified uniform mesh is used where all regular quadrature panels are given as equal lengths as possible. The mesh is uniformly refined. The number of discretization points is N. The straight line indicates seventh order convergence. Double precision arithmetic is used. The reference values are taken as $F_{\mathrm{I}} = 1.33371216025788872 79$ and $B = -1.03855893471432307225$. See Figure 7 for a quadruple precision convergence plot of F_{I}. The relative errors for values that coincide with the reference values, up to double precision accuracy, are displayed as $1.11 \cdot 10^{-16}$.

10.1 A center cracked square

First we consider a square (a rectangle with height to width ratio $h/w = 1$) with a centered crack of relative length $a/w = 0.5$ and $\theta = 0$. We use a uniform external traction of unit strength applied to the upper and lower sides of the square. The left and right sides of the square are traction-free, see Figure 4. Figure 6 illustrates the convergence of the normalized stress intensity factor F_{I} of (52) and the biaxiality parameter B of (58) under increased uniform resolution. The asymptotic convergence rate is approximately seven. The number of GMRES iterations needed for full convergence never exceeds 26. This problem is very well conditioned and in an ideal algorithm the relative error would converge to a number close to machine epsilon, which is $1.11 \cdot 10^{-16}$ in double precision accuracy. We

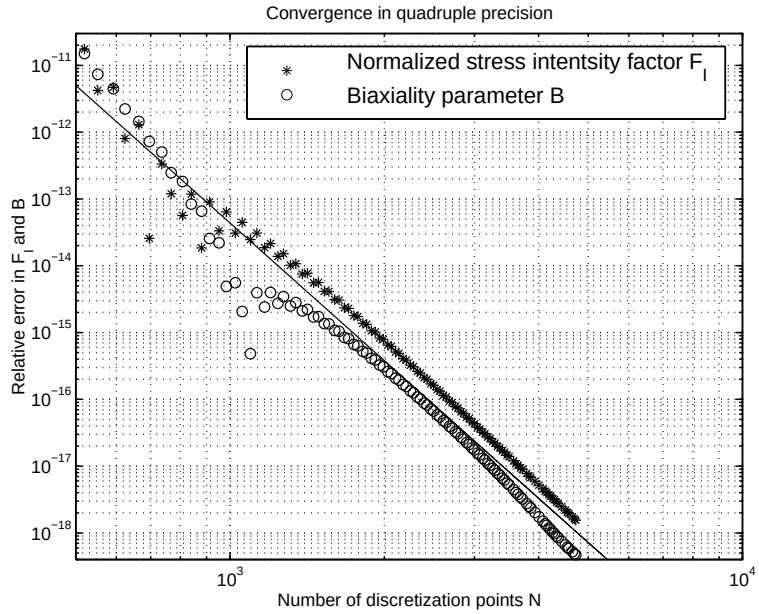

Figure 7: Quadruple precision calculations. Convergence of Stress intensity factor F_{I} of (52) and biaxiality parameter B of (58) for a centered crack of length $2a = 0.5$ in a unit square under unit uniform uniaxial load. The straight line indicates 6.845th order convergence. The reference values are taken as $F_{\mathrm{I}} = 1.33371216025788872 79$ and $B = -1.03855893471432307225$. A modified uniform mesh is used, where all regular quadrature panels are given as equal lengths as possible. The mesh is uniformly refined.

note that our algorithm is almost ideal. Figure 7 depicts convergence in quadruple precision arithmetic.

10.2 A rectangle with a slanted central crack

We now proceed to an elastic rectangle with height to width ratio $h/w = 2$ and relative crack-length $a/w = 0.6$. The crack is slanted with an angle $\theta = \pi/4$. Figure 8 illustrates the convergence of the normalized stress intensity factor F and T-stress under increased uniform resolution. This problem is just about as well conditioned as the setup with the square. The number of GMRES iterations needed for full convergence never exceeds 35. We note that, compared with the square, more discretization points are needed on the modified uniform mesh to achieve a given accuracy and the achievable accuracy is slightly lower.

10.3 A square with an arc-shaped central crack

In a third example we let the crack assume the shape of a circular arc parameterized by

$$z(t) = 0.25e^{it}\,, \qquad \pi/6 \le t \le 5\pi/6\,. \tag{63}$$

The height to width ratio of the specimen is $h/w = 1$ and uniform external traction of unit strength is applied. This problem, too, is well conditioned. The number of GMRES

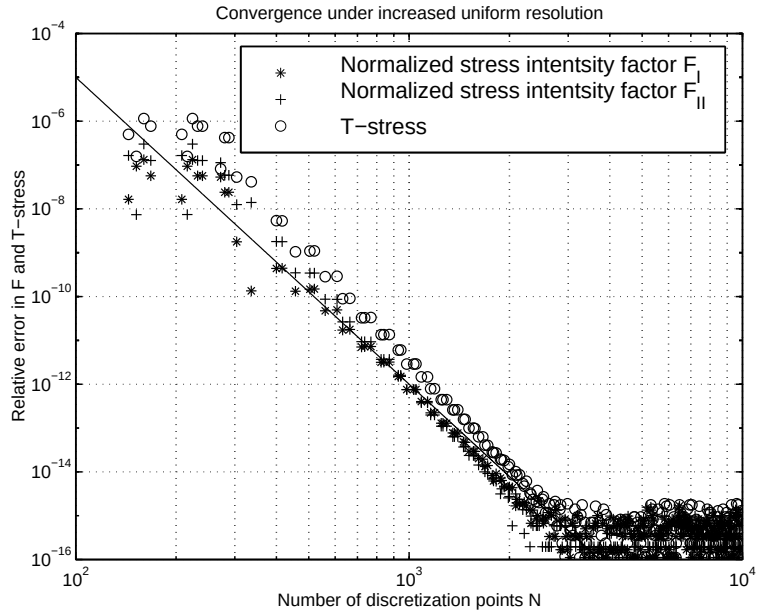

Figure 8: Convergence of normalized stress intensity factor F of (52) and a parameter given by $T\sqrt{\pi a}/K_{\mathrm{I}}$. The geometry is a rectangle with height to width ratio $h/w = 2$ and relative crack-length $a/w = 0.6$. The crack is slanted with an angle $\theta = \pi/4$, see Figure 4. The straight line indicates seventh order convergence. Double precision arithmetic is used. The reference values are taken as $F_{\mathrm{I}} = 0.66119932929855292$, $F_{\mathrm{II}} = 0.56738161111966136$, and $T\sqrt{\pi a}/K_{\mathrm{I}} = -0.23643470029373758$.

iterations needed for full convergence never exceeds 33. In Figure 9 we plot the von Mises effective stress of (48) for the case of plane strain. A Poisson's ratio of $\nu = 0.3$ is used.

Table 1: Results for the largest biaxiality parameter B and largest normalized stress intensity factors F_{I} and F_{II} in the setup of Figure. 5. The number of cracks is $4m^2$.

m	F_{I}	F_{II}	B
1	0.665322716297	0.597261470638	-0.2482174128
2	0.687185586910	0.591012369474	0.338769557
4	0.68740298100	0.59085705430	0.348567181
8	0.68735002898	0.59087320420	0.348482597
16	0.68734381100	0.59087534562	0.348590174

10.4 A square with multiple slanted cracks

Finally, a large-scale problem is studied, using the fast multipole method for evaluating matrix-vector products. We choose a setup that is easy to reproduce. A square elastic plate with side length $2w$ with $4m^2$ cracks is studied. The size of the setup is determined by

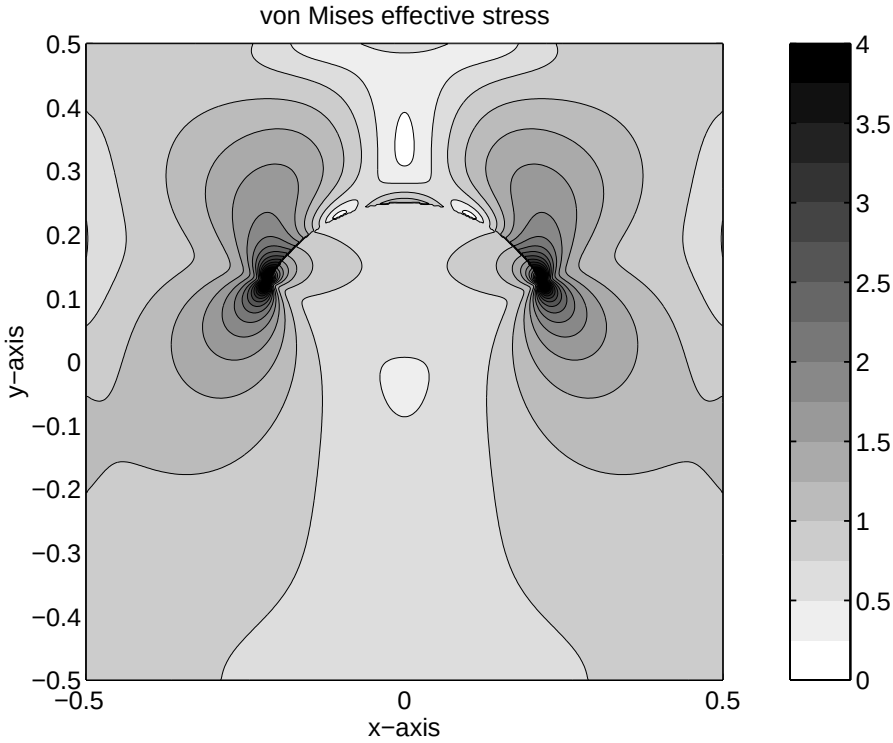

Figure 9: Distribution of von Mises effective stress of (48) in an elastic unit square containing a circular arc-shaped crack parameterized according to (63). Plane strain is assumed with Poisson's ration $\nu = 0.3$. A grid with 152,100 interior points was used for the plot.

the parameter m. The crack length is $2a = 0.6w/m$ and the cracks are slanted $\pm\pi/4$, see Figure 5. The cracks are placed in a square grid with a distance w/m between closest grid points. Due to the symmetry of geometry and load, there is a fourfold equivalence between the cracks. That is, each crack has three equivalent companions. We study the convergence of the maximum absolute values of the stress intensity factors F_{I} and F_{II} and the biaxiality parameter B, as a function of m and the number of discretization points N. In Table 1 we show how these quantities converge with the parameter m. The maximum absolute values of F_{I} and F_{II} occur at the cracks closest to the corners of the square plate for all values of m. The maximum values of F_{I} occur at the crack-tips closest to the sides where the load is applied, while the maximum absolute values of F_{II} occur at the crack-tips closest to the sides which are traction-free. The minimum values of B, which are negative, occur at the cracks closest to the corners for all m, at the crack-tips closest to the sides where the load is applied. The maximum B, which is positive, occurs at the second and last-but-one cracks in the second and last-but-one rows of cracks, counting from the boundaries for $m \geq 2$. Since for $m = 1$ only the cracks closest to the corners are present, B of Table 1 is negative for $m = 1$ and positive for $m \geq 2$. The results for $m = 1$ are quite similar to the results for one slanted crack of Section 10.2. From Table 1 it can be noted that B converges slower with m than F_{I} and F_{II}, indicating that B is more sensitive to the geometry than the stress intensity factors are. Since B is negative at the crack-tips where F_{I} attains its maxima,

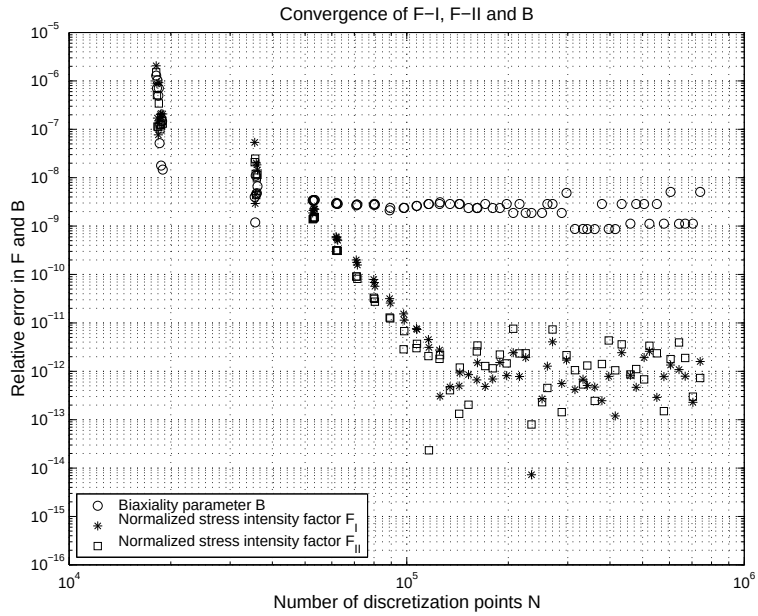

Figure 10: Convergence of the maximal normalized stress intensity factors F_{I} and F_{II} and the maximal biaxiality parameter B. The geometry is a square with 1024 slanted cracks, se the right image of Figure 5. Double precision arithmetic is used. Up to 740,000 discretization points are placed on the boundary. The fast multipole method is used for matrix-vector multiplication. The reference values are taken as $F_{\mathrm{I}} = 0.687343811003354$, $F_{\mathrm{II}} = 0.590875345620499$, and $B = 0.348590174271453$ About 50 GMRES iterations are needed for full convergence.

a fracture criterion accounting for T-stress effects would be needed for failure prediction in this case, as discussed in Section 5. The largest setup studied contains 1024 cracks, corresponding to $m = 16$. For this setup we also show the convergence of F_{I}, F_{II} and the biaxiality parameter B, as a function of the number of discretization points, see Figure 10. While F_{I} and F_{II} converge to a relative precision better than 10^{-11}, B only converges down to about 10^{-9}. There might be several reasons for this. While the stress intensity factors corresponds to the first terms in the series expansion of the stress field, B corresponds to the second, constant, term in the expansion for σ_{xx}. The first terms might in some sense be easier to compute than higher order terms.

11 DISCUSSION

We have constructed and implemented a seventh order accurate solver for the computation of stress fields inside cracked rectangular domains. We have demonstrated the extreme stability of the solver and we have extracted useful quantities from the solution. Our algorithm is efficient. In Section 10.1, with only 112 discretization points and less than 10 seconds of computing time on a workstation, we computed normalized stress intensity factors and biaxiality parameters for a simple setup as accurately as an engineer could possibly require. A number of 112 discretization points corresponds to the coarsest mesh we can construct without substantially violating the rules for the placement of quadrature

Table 2: Numerical results for the biaxiality parameter B and the normalized stress intensity factor F_{I} of a centrally cracked specimen with $\theta = 0$, and with different ratios h/w and a/w, see Figure 4. Three stars indicate that no value was presented. The symbols (t), (g), and (i) indicates tabulated, graphical, and interpolated data. (1) Leevers and Radon (1982) claim four digit agreement with Isida (1971). (2) The specimen in (Mukhopadhyay *et al.* (1998)) is intended as infinite, but a ratio $h/w = 5$ was used for the numerical results (Mukhopadhyay, private communication).

h/w	a/w	B	F_{I}	ref	
1	0.3	$***$	1.123	Isida (1971)	(t)
1	0.3	-1.03	$1.123^{(1)}$	Leevers, Radon (1982)	(i)
1	0.3	-1.032	$***$	Cardew *et al.* (1984)	(t)
1	0.3	-1.02	1.12	Kfouri (1986)	(g)
1	0.3	-1.03	1.12	Fett (1998)	(t)
1	0.3	$***$	1.1214	Kabele *et al.* (1999)	(t)
1	0.3	-1.0286	1.1232	Chen *et al.* (2001)	(t)
1	0.3	-1.02864238631710	1.12319110266148	new	
1	0.5	$***$	1.3337	Isida (1971)	(t)
1	0.5	-1.04	$***$	Larsson, Carlsson (1973)	(t)
1	0.5	-1.04	$1.334^{(1)}$	Leevers, Radon (1982)	(i)
1	0.5	-1.039	$***$	Cardew *et al.* (1984)	(t)
1	0.5	$***$	1.331	Banks-Sills, Sherman (1986)	(t)
1	0.5	-1.02	1.31	Kfouri (1986)	(g)
1	0.5	$***$	1.331	Banks-Sills, Sherman (1992)	(t)
1	0.5	$***$	1.3341	Chan, Mear (1995)	(t)
1	0.5	$***$	1.3296	Zhu, Smith (1995)	(t)
1	0.5	-1.04	1.33	Fett (1998)	(t)
1	0.5	$***$	1.3317	Kabele *et al.* (1999)	(t)
1	0.5	$***$	1.332	Guinea *et al.* (2000)	(t)
1	0.5	-1.0385589347143231	1.3337121602578887	new	
∞	0.6	$***$	1.3033	Isida (1973)	(i)
3	0.6	$***$	1.32548	Gu (1993)	(t)
3	0.6	-1.11408542438965	1.30332730119436	new	
∞	0.8	$***$	1.8160	Isida (1973)	(i)
$5^{(2)}$	0.8	$***$	1.7577	Mukhopadhyay *et al.* (1999)	(t)
5	0.8	-1.41111943705804	1.8159948204573	new	

panels, presented in Section 7. Incorporating the fast multipole method into the solver makes it possible to treat large-scale problems. In Section 10.4, stress intensity factors and biaxiality parameters for a setup containing up to 1024 cracks are computed with a relative precision better than 10^{-8}.

One may argue that fast and stable solvers for linear fracture mechanics problems are not needed. After all, most computational problems of engineering importance are non-linear.

Table 3: Results for the parameter $T\sqrt{\pi a}/K_{\mathrm{I}}$ and the normalized stress intensity factors F_{I} and F_{II} of a centrally cracked specimen with $h/w = 2$ and $a/w = 0.6$. The crack is slanted with an angle $\theta = \pi/4$. Three stars indicate that no values were presented. (1) Different values are presented. Mean value of best calculations is quoted.

$T\sqrt{\pi a}/K_{\mathrm{I}}$	F_{I}	F_{II}	ref
* * *	0.6611	0.5674	Kitagawa, Yuuki (1977)
* * *	0.659	0.568	Murakami (1978)
* * *	0.666	0.569	Portela *et al.* (1992)
* * *	$0.669^{(1)}$	$0.562^{(1)}$	Sáez (1995)
* * *	0.6636	0.5706	Mukhopadhyay *et al.* (1998)
−0.2248	0.654	0.567	Yang B, Ravi-Chandar (1999)
* * *	0.6609	0.5660	Kebir *et al.* (1999)
* * *	$0.665^{(1)}$	$0.581^{(1)}$	Murthy, Mukhopadhyay (2001)
−0.23643470029374	0.66119932929855	0.56738161111966	new

High accuracy is seldom required. Fast algorithms are unnecessary since the computers themselves become faster all the time. Our answer to such criticism now follows:

First, highly accurate values of stress intensity factors and biaxiality parameters for a vast number of topologies can now be computed in seconds. This paper treats interior cracks in finite domains. In previous work we have presented equally stable algorithms for the computation of stress intensity factors for cracks in infinite and periodic domains (see Helsing and Peters(1999)), for interface cracks (see Helsing (1999)) in infinite domains, and for notches in finite domains (see Helsing and Jonsson (2001)). This means that we approach a situation where one can replace the use of tables, in the laboratory or in a design process, with the use of software. The use of reliable software will enable the engineer to check a wider range of geometric parameters than a table could ever cover.

Second, fast computers alone are not sufficient to produce better solutions for solid mechanics problems. One needs more efficient algorithms too. This is illustrated in Table 2 and in Table 3 where our new results are placed in a historic setting. A fact, which can be observed in these tables, is that the oldest numerical results for F, those of Isida (1971) and Kitagawa and Yuuki (1977), have higher quality in terms of accuracy than many of the newer results. For slender specimens, a thirty year old interpolation formula, see Isida (1973), gives the most reliable results. This is remarkable, considering the enormous progress that has been made in the area of scientific computing during the last decades.

Third, fast and stable linear solvers are needed as fundamental building blocks in more complex solvers which, for example, can simulate micro-crack evolution in composite materials on their way from crack initiation to macroscopic failure, or treat problems involving plasticity. High accuracy may not be required in the final answer, but stability is a crucial property – especially when dealing with non-linear equations and complex geometries where cracks may lie close to each other and to the boundary of the specimen. Realistic setups are not as simple as the one depicted in Figure 4 which is the most studied geometry in the literature. When we refine the mesh we must be absolutely confident that the error becomes

smaller. Otherwise predicted crack-patterns will become mesh-dependent and the numerical procedure is useless as a design tool. Demonstrated ability to achieve high accuracy for non-trivial examples serves as a numerical proof of that an algorithm is stable.

References

[1] ASTM E 399 – Standard Test Method for Plane-Strain Fracture Toughness of Metallic Materials, in Annual Book of ASTM Standards, Section 3 Metals Test Methods and Analytical Procedures. ASTM: West Conshohocken, 1998, 413–443.

[2] Banks-Sills L, Sherman D. Comparison of methods for calculating stress intensity factors with quarter point elements. *International Journal of Fracture* 1986; **32**:127–140.

[3] Banks-Sills, L, Sherman D. On the computation of stress intensity factors for 3-dimensional geometries by means of the stiffness derivate and J-integral methods. *International Journal of Fracture* 1992; **53**:1–20.

[4] Becker AA. *The boundary element method in engineering.* McGraw-Hill: London, 1992.

[5] Betegón C, Hancock JW. Two-Parameter Characterization of Elastic-Plastic Crack-Tip Fields. *ASME Journal of Applied Mechanics* 1991; **58**:104–110.

[6] Cardew GE, Goldthorpe MR, Howard IC, Kfouri AP. *On the elastic T-term, in Fundamentals of Deformation and Fracture.* Bilby BA, Miller KJ, Willis JR, ed., Cambridge University Press: Cambridge, 1984, 465–476.

[7] Chang C, Mear ME. A boundary element method for two dimensional linear elastic fracture analysis. *International Journal of Fracture*; 1995; **74**:219–251.

[8] Chen CS, Krause R, Pettit RG, Banks-Sills L, Ingraffea AR. Numerical assessment of T-stress computation using a p-version finite element method. *International Journal of Fracture*; 2001; **107**:177–199.

[9] Estrada R, Kanwal RP. *Singular Integral Equations.* Birkhäuser: Boston, 2000.

[10] Fett T. T-stresses in rectangular plates and circular disks. *Engineering Fracture Mechanics* 1998; **60**:631–652.

[11] Greengard L, Helsing J. On the numerical evaluation of elastostatic fields in locally isotropic two-dimensional composites. *Journal of the Mechanics and Physics of Solids* 1998; **46**(8):1441–1462.

[12] Greengard L, Rokhlin V. A fast algorithm for particle simulations, *Journal of Computational Physics* 1987; **73**):325–348.

[13] Gu L. A compatible boundary element method for plane elasticity and fracture mechanics. *Applied Mathematical Modelling* 1993; **17**:394–405.

[14] Guinea GV, Planas J. Elices M. K_{I} evaluation by the displacement extrapolation technique. *Engineering Fracture Mechanics* 2000; **66**:243–255.

[15] Hallbäck N, Jönsson N. T-stress evaluations of mixed mode I/II fracture specimens and T-effects on mixed mode failure of aluminium. *International Journal of Fracture* 1996; **76**:141–168.

[16] Helsing J. On the numerical evaluation of stress intensity factors for an interface crack of a general shape. *International Journal for Numerical Methods in Engineering* 1999; **44**(5):729–741.

[17] Helsing J. On the interior stress problem for elastic bodies. *ASME Journal of Applied Mechanics* 2000; **67**(4):658–662.

[18] Helsing J, Jonsson A. On the computation of stress fields on polygonal domains with V-notches. *International Journal for Numerical Methods in Engineering* 2002; **53**(2): 433–453.

[19] Helsing J, Peters G. Integral equation methods and numerical solutions of crack and inclusion problems in planar elastostatics. *SIAM Journal on Applied Mathematics* 1999; **59**(3):965–982.

[20] Higham NJ. *Accuracy and stability of numerical algorithms.* SIAM: Philadelphia, 1996, 92–97.

[21] Isida M. Effect of Width and Length on Stress Intensity Factors of Internally Cracked Plates Under Various Boundary Conditions. *International Journal of Fracture Mechanics* 1971; **7**:301–316.

[22] Isida M. Analysis of stress intensity factors for the tension of a centrally cracked strip with stiffened edges. *Engineering Fracture Mechanics* 1973; **5**:647–665.

[23] Kabele P, Yamaguchi E, Horii H. FEM-BEM superposition method for fracture analysis of quasi-brittle structures. *International Journal of Fracture* 1999; **100**:249–274.

[24] Kebir H, Roelandt JM, Foulquier J. A new singular boundary element for crack problems – Application to bolted joints. *Engineering Fracture Mechanics* 1999; **62**:497–510.

[25] Kahan W. Further remarks on reducing truncation errors. *Communications of the Association for Computing Machinery* 1965; **8**:40.

[26] Kitagawa H, Yuuki R. Analysis of arbitrarily shaped crack in a finite plate using conformal mapping, 1st report - construction of analysis procedure and its applicability. *Transactions of the Japanese Society of Mechanical Engineers* 1977; **43**:4354–4362.

[27] Kfouri AP. Some evaluations of the elastic T-term using Eshelby's method. *International Journal of Fracture* 1986; **30**:301–315.

[28] Larsson SG, Carlsson AJ. Influence of non-singular stress terms and specimen geometry on small-scale yielding at crack tips in elastic-plastic materials. *Journal of the Mechanics and Physics of Solids* 1973; **21**:263–277.

[29] Leevers PS, Radon JC. Inherent stress biaxiality in various fracture specimen geometries. *International Journal of Fracture* 1982; **19**:311–325.

[30] Mikhlin SG. *Integral equations.* Pergamon Press: London, 1957.

[31] Mukhopadhyay NK, Maiti SK, Kakodkar A. BEM based evaluation of SIFs using modified crack closure integral technique under remote and/or crack edge loading. *Engineering Fracture Mechanics* 1998; **61**:655–671.

[32] Mukhopadhyay NK, Maiti SK, Kakodkar A. Effect of modelling of traction and thermal singularities on accuracy of SIFS computation through modified crack closure integral in BEM. *Engineering Fracture Mechanics* 1999; **64**:141–159.

[33] Murakami Y. Application of the body force method to the calculation of stress intensity factors for a crack in the arbitrarily shaped plate. *Engineering Fracture Mechanics* 1978; **10**:497–513.

[34] Murthy KSRK, Mukhopadhyay M. Adaptive finite element analysis of mixed-mode fracture problems containing multiple crack-tips with an automatic mesh generator. *International Journal of Fracture* 2001; **108**:251–274.

[35] Muskhelishvili NI. *Some Basic Problems of the Mathematical Theory of Elasticity.* P. Noordhoff Ltd: Groningen, 1953.

[36] Muskhelishvili NI. *Singular Integral Equations.* P. Noordhoff Ltd: Groningen, 1953.

[37] Parton VZ, Perlin PI. *Integral Equation Methods in Elasticity.* MIR: Moscow, 1982.

[38] Parton VZ, Perlin PI. *Mathematical Methods of the theory of Elasticity.* MIR: Moscow, 1984.

[39] Portela A, Aliabadi MH, Rooke DP. The dual boundary element method: effective implementation for crack problems. *International Journal for Numerical Methods in Engineering* 1992; **33**:1269–1287.

[40] Saad Y, Schultz MH. GMRES: a generalized minimum residual algorithm for solving nonsymmetric linear systems. *SIAM Journal on Scientific and Statistical Computing* 1986; **7**:856–869.

[41] Sáez A, Gallego R, Domínguez J. Hypersingular quarter-point boundary elements for crack problems. *International Journal for Numerical Methods in Engineering* 1995; **38**:1681–1701.

[42] Sokolnikoff IS. Mathematical Theory of Elasticity, McGraw-Hill, New York, 1956.

[43] Williams ML. Stress singularities resulting from various boundary conditions in angular corners of plates in extension. *ASME Journal of Applied Mechanics* 1952; **19**:526–528.

[44] Yang B, Ravi-Chandar K. Evaluation of elastic T-stress by the stress difference method. *Engineering Fracture Mechanics* 1999; **64**:589–605.

[45] Zhu WX, Smith DJ. On the use of displacement extrapolation to obtain crack tip singular stresses and stress intensity factors. *Engineering Fracture Mechanics* 1995; **51**:391–400.